JOURNAL OF PROPULSION AND POWER
Vol. 10, No. 1, Jan.–Feb. 1994

Theoretical Study of Sensor-Actuator Schemes for Rotating Stall Control

G. J. Hendricks* and D. L. Gysling†
Massachusetts Institute of Technology, Cambridge, Massachusetts 02139

A theoretical study has been conducted to determine the influence of actuator and sensor choice on active control of rotating stall in axial-flow compressors. The sensors are used to detect small amplitude traveling waves that have been observed at the inception of rotating stall in several different compressors. Control is achieved by feeding the sensed quantity back to the actuator with a suitable gain and spatial phase shift relative to the measured wave. Actuators using circumferential arrays of jets, intake ports, and movable inlet guide vanes upstream of the compressor, and valves downstream of the compressor were considered. The effect of axial velocity, static pressure, or total pressure measurement on control effectiveness was investigated. In addition, the influence of the actuator bandwidth on the performance of the controlled system was determined. The results of the study indicate that the potential for active control of rotating stall is greater than that achieved thus far with movable inlet guide vanes. Furthermore, axial velocity sensing was most effective. Actuator bandwidth affected the performance of the controlled compressors significantly, but certain actuators were affected less severely than others.

Nomenclature

$\bar{L}_r$ = steady total pressure loss across rotors
$\bar{L}_s$ = steady total pressure loss across stator
l_a = compressor annulus height
n = spatial harmonic number
P_{ti} = inlet total pressure
R = feedback gain
r = compressor annulus mean radius
s = $(\alpha_n + i\omega_n)r/U$
t = time
$\bar{t}$ = nondimensional time tU/r
Z = complex feedback gain $Re_a^{i\vartheta}$
α = disturbance growth rate
δL_r = perturbation in total pressure loss across rotors
δL_s = perturbation in total pressure loss across stators
δl_j = jet valve opening
δP_e = exit static pressure perturbation
δP_i = inlet static pressure perturbation
δP_{ti} = inlet total pressure perturbation
$\delta\phi$ = flow coefficient perturbation
ϑ = circumferential coordinate
ϑ_a = feedback spatial phase shift
λ = inertia parameter for compressor rotors
μ = inertia parameter for compressor
ρ = fluid density
$\bar{\tau}_a$ = nondimensional actuator time constant
$\bar{\tau}_r$ = nondimensional rotor total pressure loss characteristic time
$\bar{\tau}_s$ = nondimensional stator total pressure loss characteristic time
ϕ = flow coefficient c_x/U
ψ = total-to-static pressure rise
ψ_i = ideal (isentropic) total-to-static pressure rise
$\bar{\psi}$ = steady-state total-to-static pressure rise
ω = disturbance rotational frequency
ω_r = rotor rotational frequency

Presented as Paper 92-3486 at the AIAA/SAE/ASME/ASEE 28th Joint Propulsion Conference, Nashville, TN, July 6–8, 1992; received Sept. 8, 1992; revision received June 4, 1993; accepted for publication June 7, 1993.

*Postdoctoral Associate, Gas Turbine Laboratory. Member AIAA.
†Graduate Student, Gas Turbine Laboratory.

Introduction

AXIAL flow compressors suffer fluid dynamic instabilities known as surge and rotating stall. Surge involves the entire compression system, while rotating stall is local to the compressor and is characterized by a region of stalled flow rotating about the annulus of the compressor. This study addresses active control of rotating stall.

When rotating stall is encountered in the compressor of a gas turbine engine, the pressure rise across the compressor drops abruptly, resulting in a significant decrease in the power output of the engine. In addition, engine health is affected adversely by large fluctuating loads that are induced on the compressor blades. The compressor of a gas turbine engine is therefore normally operated far enough away from the stall inception point so that instability is not triggered under any operating condition. This margin of safety is known as the stall margin. Because rotating stall is normally encountered close to the peak of the pressure-rise characteristic of the compressor, the stall margin places a limit on both the performance and operating range of the engine. An actively controlled compressor could operate stably past the peak of the pressure rise characteristic. With the same stall margin as in the uncontrolled case, the peak of the characteristic could then be a safe operating point.

Active control of rotating stall studied here is based on a linear model of its initiation. The model implies that, at the inception of the instability, small amplitude, long wavelength, traveling waves develop in the compressor annulus, grow in magnitude, and eventually develop into rotating stall cells.[1–3] Although such small amplitude waves have not been observed in all situations, they are a clear feature of recent tests on several compressors of widely different geometry.[4,5,7–9] In some compressors, disturbances with wavelengths of the order of the blade pitch are observed prior to stall.[6] These disturbances have a three-dimensional structure. The present study which assumes that the disturbances are two-dimensional (i.e., no radial variation) might therefore not apply to compressors in which these short wavelength disturbances are observed.

The correspondence observed so far between linear fluid dynamic analysis and experimental observations is encour-

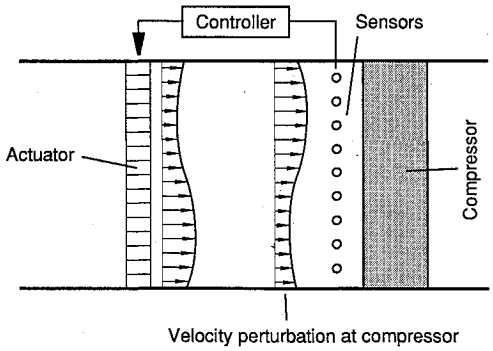

Fig. 1 Compressor with actuator and sensors.

aging since it gives one confidence in using the theory to design devices which can be used to modify the inlet and/or exit flowfields of the compressor in order to suppress the instability. These controlling devices would act in the inception phase of the instability before it develops to its performance limiting amplitude. The controllers that will be described in this study are therefore designed to prevent the compressor from going into rotating stall when the system is operated within the parameters of the controller.

A schematic diagram of a conceptual controlled system is shown in Fig. 1. A fluid dynamic variable which gives an indication of the magnitude and form of the instability is sensed by a suitable array of transducers. The signal from the transducer array is processed by the controller which commands the actuator to introduce a suitable control disturbance into the flowfield. Initial studies of this problem[3] have considered only simple control strategies, e.g., actuators which introduce a vortical velocity perturbation at the compressor inlet plane (a model for movable guide vanes far upstream of the compressor). The use of close coupled movable inlet guide vanes for the control of rotating stall has been demonstrated experimentally by Paduano[7,8] and Haynes[9] (the stalling mass flow rate was decreased by 23% in the experiment on a single-stage compressor,[7,8] and 8% on a three-stage unit[9]). The objective of the present study is to examine the potential for increasing the system controllability, in particular to assess the effectiveness of a number of different sensing and actuation devices.

Analytical Model

Overall Considerations

The analytical model used in this study is an extension of that described in Refs. 1–3. The analysis is two dimensional, so only high hub-to-tip ratio machines are considered. The mean inlet flowfield is undistorted (uniform inlet total pressure), and the inlet and exit ducts are assumed long, so that end effects (i.e., reflection and scattering of the disturbance wave from the ends) are not important. In addition, the tip speed of the compressor is assumed to be low enough for the flowfield to be considered incompressible. In the analysis an arbitrary axial velocity disturbance wave is decomposed into its spatial Fourier harmonics:

$$\delta\phi = \sum_{n=1}^{\infty} A_n e^{st} e^{in\vartheta}$$

where

$$s = \frac{(\alpha_n + i\omega_n)r}{U}$$

In the above formulation $\omega_n r/nU$ represents the rotation rate of each spatial harmonic nondimensionalized by the rotor rotational speed, and $\alpha_n r/U$ the nondimensionalized growth rate of the disturbance. The spatial harmonics, which are the natural eigenmodes of the system, can then be analyzed independently, since the equations describing the evolution of the instability are linear. When the above form of the flow coefficient perturbation is substituted into the differential equations describing the dynamics of the fluid in the compression system, the analysis yields an eigenvalue problem in s with the growth and rotation rates of each spatial harmonic determined from the solution to the eigenvalue problem. If the real part of s is negative, the disturbance is damped, representing stable operation of the compressor; if the real part of s is positive, the disturbance grows exponentially, representing unstable operation.

If the compressor is assumed to operate in a quasisteady manner (i.e., pressure rise is a function of flow coefficient only), the model predicts that all the spatial harmonics of the flow coefficient perturbation become unstable at the operating point where the total-to-static pressure-rise characteristic (ψ vs ϕ) becomes positively sloped. Disturbances are damped where the characteristic is negatively sloped, and amplified when the characteristic is positively sloped, with the growth rate of the perturbation being determined by the magnitude of the positive slope. In the formulation of the model used in the present study, the quasisteady assumption is not made.

Unsteady Compressor Behavior

It has been observed in experiments[10,11] that the pressure rise across a compressor does not respond instantaneously to variations in flow coefficient. This is thought to be a result of the finite time required for the flowfields within the blade passages to respond to changes in flow coefficient. The finite response time of the compressor pressure-rise to flow perturbations has a stabilizing effect on the perturbations, and higher harmonics are stabilized to a greater extent than lower harmonics. When this effect is included in the analysis, the spatial harmonics of the disturbance become unstable sequentially, with higher harmonic disturbances becoming unstable at larger positive slopes of the compressor total-to-static pressure-rise characteristic (i.e., lower flow coefficients). This behavior has been observed in experiments on both single- and three-stage low-speed compressors,[7–9] and the model shows good quantitative agreement with experiments conducted on a three-stage compressor.[9,12] The sequential destabilization of higher spatial harmonics of flow coefficient disturbances has beneficial implications for active control. By controlling only the first spatial harmonic of the disturbance, an increase in stable operating range can be obtained, down to the flow coefficient at which the second spatial harmonic of the disturbance becomes unstable. By controlling both the first and second spatial harmonics beyond this flow coefficient, the stable operating range can then be extended to the operating point where the third spatial harmonic becomes unstable. Using this control approach, the maximum range extension possible is therefore dependent on the number of spatial harmonics of the disturbance that one is able to control.

It has been mentioned earlier that the slope of the compressor pressure rise characteristic $d\psi/d\phi$, is an important parameter governing the growth rate of a disturbance wave. The pressure-rise characteristic (shown later in Fig. 13), which has a slope going to an infinite positive value at a flow coefficient of 0.25, is used in the computations described below since it covers all positive slopes that could be encountered in practice.

Actuators and Sensors

In this study only actuators that are close coupled with the compressor are considered. This eliminates the time delay associated with the convection of the vortical component of the control disturbance from the actuator to the compressor, which was found to have a destabilizing effect on the system. Actuators can be considered close coupled if they are posi-

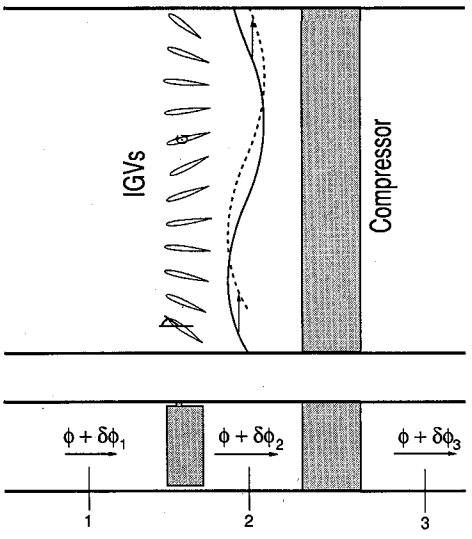

Fig. 2 Inlet guide vane actuator.

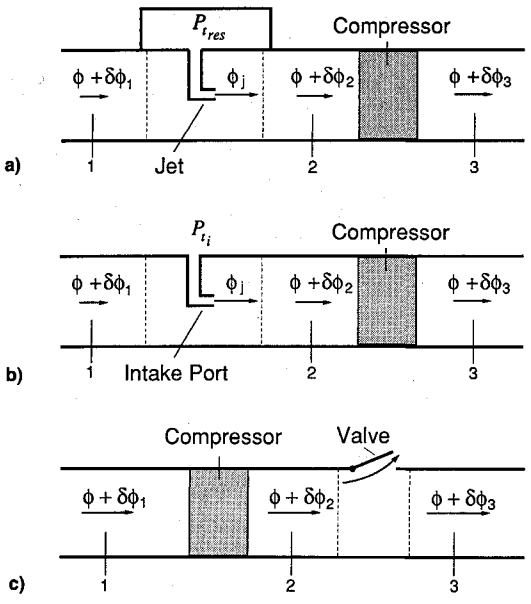

Fig. 3 Schematic diagrams of: a) jet actuator, b) intake port actuator, and c) valve actuator.

tioned a distance smaller than the disturbance wavelength from the compressor inlet or exit plane.

The following actuators are considered: 1) movable inlet guide vanes upstream of the compressor, 2) jets upstream of the compressor, 3) intake ports upstream of the compressor, and 4) valves downstream of the compressor. This is not a complete list, but the actuators considered show the performance variations that one could expect in selecting an actuator. The actuators are shown schematically in Figs. 2 and 3. The intake port and jet actuators are similar physically, but they differ in the supply pressure to the actuator. The jet actuator is supplied by a high-pressure reservoir, whereas the intake port actuator is supplied by a reservoir having the same total pressure as the compressor inlet. In the study, the reservoir of the jet actuator is supplied by the exit of the compressor, so the reservoir stagnation pressure is set equal to the exit static pressure at the compressor operating point. The intake port actuator does not require such a high-pressure air supply; fluid at the total pressure of the inlet air can be derived from the freestream outside the compressor casing. (Gysling[13] has identified the jet distribution as an effective actuator in a similar study on control of rotating stall using aeromechanical feedback.) The movable inlet guide vane actuator has already been implemented experimentally by Paduano[7,8] and Haynes,[9] and is used as a basis for comparison for the other actuators. These experiments have also served as a validation of the modeling technique used in the study.

In the uncontrolled compression system the relation between flow coefficient and pressure perturbations at the compressor inlet and exit planes is determined by the dynamics of the fluid in the compressor, and in the inlet and exit ducts of the compressor. Under active control these relations can be manipulated by the actuator. In the analysis done for this study the actuators are modeled using quasisteady actuator disk theory. The last aspect of the analysis involves sensing a fluid dynamic variable, and prescribing a feedback law between the sensed variable and the actuation. Only the following proportional feedback law is considered in this article:

$$\text{actuation} = Z \times \text{sensed variable}$$

where

$$Z = Re^{i\vartheta_a}$$

R is the gain in amplitude of the sensed variable, and ϑ_a the circumferential spatial phase shift of the actuated wave relative to the sensed wave. In the study, the gain and spatial phase of the feedback signal are optimized for various compressor operating conditions.

In practice, the output of the actuator will differ from the command given by the controller. To capture this nonideal behavior, the actuator is modeled as a first-order time-lag system:

$$\bar{\tau}_a \frac{\mathrm{d}(\text{actuation})}{\mathrm{d}\bar{t}} = \text{command} - \text{actuation}$$

A time lag $\bar{\tau}_a$ is assumed between the actuation and the command given by the controller. The inverse of this time constant, $1/\bar{\tau}_a$ represents the bandwidth of the actuator.

When the feedback law and actuator dynamics are coupled to the compressor dynamics, a new eigenvalue problem is generated, with the eigenvalues of the system, i.e., the growth rate and frequency of the disturbance, dependent on the gain and phase of the feedback signal. The effect of nonideal behavior of the actuator on the system performance can be assessed by varying the time constant associated with the actuation (varying the bandwidth of the actuator). These effects are described in the next section.

Sensors measuring the following flow variables are evaluated: 1) axial velocity, 2) static pressure, and 3) stagnation pressure. A comparative study was done with the sensors positioned at various axial stations in the compression system; upstream of the actuator, between the actuator and the compressor, and downstream of the compressor. The performance of the controlled systems are reported only with the sensors located at the axial stations where they perform most favorably.

A detailed analysis of the compression system coupled with the jet actuator is given in Appendices A and B. Analysis of the inlet guide vane actuator is based on the model developed by Paduano et al.[7,8]

Calculated Results and Discussion

Influence of Actuator Type

Figures 4–7 present neutral stability curves for the first harmonic of the disturbance wave. The results for the higher spatial harmonics show trends similar to those for the first harmonic. The figures show the maximum compressor slope ($\mathrm{d}\psi/\mathrm{d}\phi$) at which stabilization can be achieved, as a function of controller gain for the four actuators considered. The areas below the neutral stability curves represent stable operation of the controlled system. For the jet, intake port, and valve

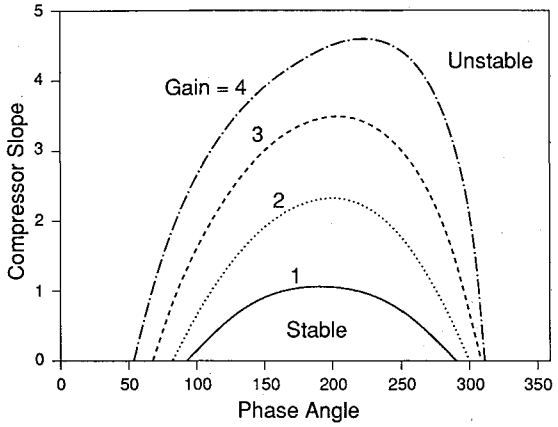

Fig. 4 Jet actuator; compressor slope at neutral stability as a function of feedback gain and phase. The system is stable in the area under the curves.

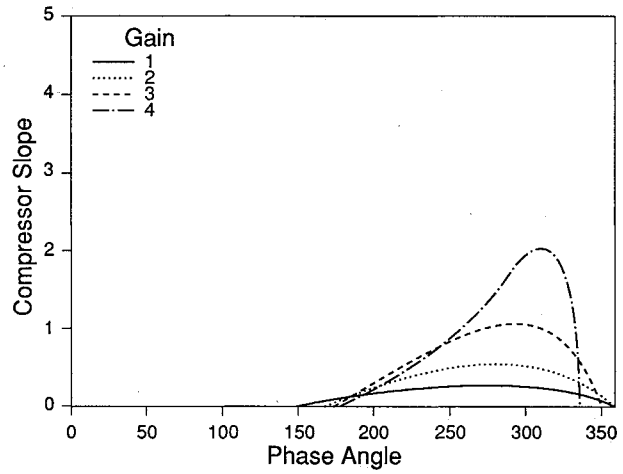

Fig. 5 Intake port actuator; compressor slope at neutral stability as a function of feedback gain and phase. The system is stable in the area under the curves.

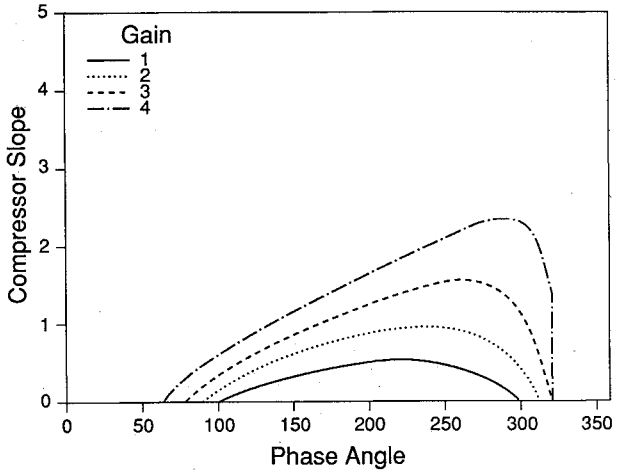

Fig. 6 Downstream valve actuator; compressor slope at neutral stability as a function of feedback gain and phase. The system is stable in the area under the curves.

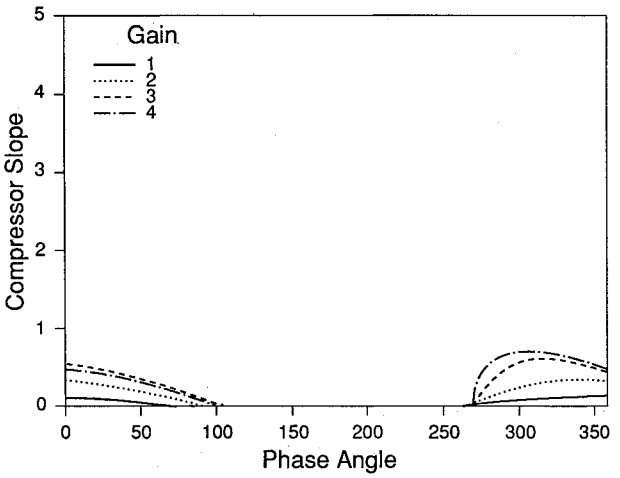

Fig. 7 Inlet guide vane actuator; compressor slope at neutral stability as a function of feedback gain and phase. The system is stable in the area under the curves.

actuators, gain is defined as the ratio of the nondimensionalized mass flow added to, or removed from the flowfield, and the sensed variable (velocity, static pressure, or stagnation pressure as indicated in Appendix B). For the movable inlet guide vane actuator, the gain is defined as the ratio of the deflection angle (in radians) of the inlet guide vanes from their zero positions, and the sensed variable.

In each case the performance of the controlled system is shown with the best sensor located at its optimum axial station (in all cases sensing the axial velocity perturbation through the compressor gave the best results). The horizontal axis in the figures represents the spatial phase shift between the measured disturbance and the actuation, and the vertical axis shows the slope of the compressor total-to-static pressure rise characteristic. Only positive compressor slopes are shown, so the figure represents an operating range that was previously inaccessible to the uncontrolled compressor. The analysis was also performed for negative characteristic slopes; this indicated that the control system could destabilize a naturally stable compression system for certain phases of the controller.

To facilitate comparison, the neutral stability curves for the four actuators operating at a gain of four are plotted on the same axes in Fig. 8. This gain was used for comparison since all the actuators showed unstable behavior for certain phases above this value. An experiment on a three-stage compressor[9] also showed that the performance of the system was degraded for gains above four.

It should be noted that the performance of the inlet guide vane actuator is influenced by the "swirl sensitivity" of the compressor, i.e., the rate of change of pressure rise across the compressor with inlet guide vane deflection. The swirl sensitivity of the three-stage compressor on which the experiment was performed[9] was used in the analysis since it was thought to be representative of practical compressors. Swirl sensitivity is determined primarily by the rate of change of the pressure rise with inlet guide vane deflection in the first stage, since the inlet angles to the rotors of the downstream stages are not affected significantly by inlet guide vane deflection. It is therefore not dependent on the number of stages of the compressor, if the geometric configuration of the first stage is similar.

Three performance parameters that are important in comparing the various actuation systems are 1) the largest positive compressor slope that the controlled system can achieve, this gives a measure of the range extension provided by the actuation system; 2) the phase margin of the controller, which gives a measure of the range of phases over which the controlled system is stable at a particular operating point; and 3) the rotation rate of the controlled perturbation. Under active control both the growth and rotation rates of the flow perturbation are modified. The rotation rate of the controlled disturbance is important since it is one of the parameters that

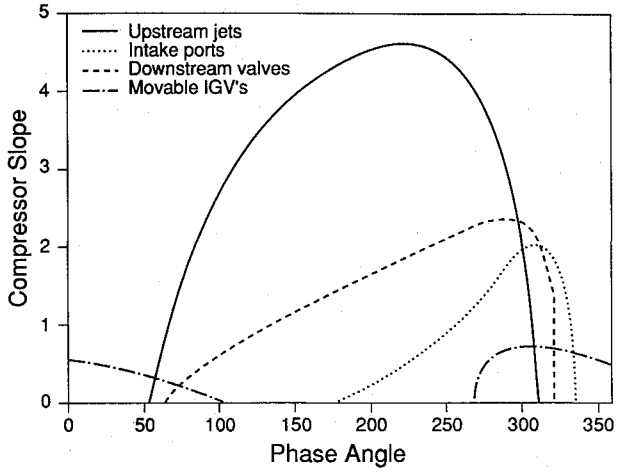

Fig. 8 Comparison of actuation schemes; velocity sensing, gain = 4.

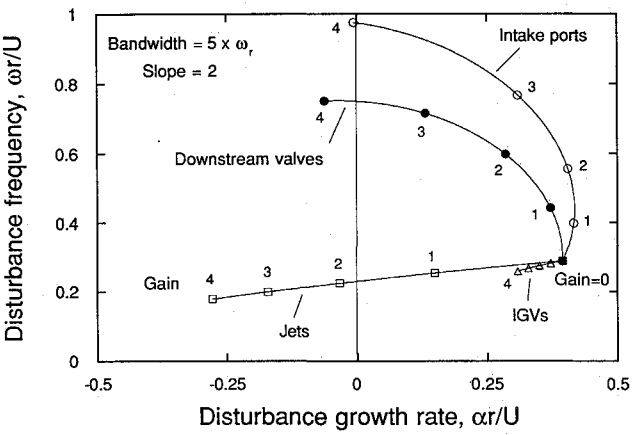

Fig. 9 Perturbation growth and rotation rates at the optimum phase for each system.

determines the bandwidth requirement of the actuator. An actuator that increases the rotation rate of the perturbation is undesirable.

From Fig. 8 it is apparent that the upstream jet distribution delivers the most favorable performance. In addition to providing the highest degree of range extension, the jet distribution also has the largest phase margin at a fixed operating point. For example, at a compressor slope of 1, the jet distribution stabilizes the compressor over a phase range of 250 deg, as opposed to 100 deg for the intake port distribution, and approximately 190 deg for the downstream valves. The movable inlet guide vanes cannot stabilize the compressor at any phase at this slope.

Figure 9 shows the change in the growth and rotation rates of the first spatial harmonic of a disturbance in the individual controlled systems, at the optimum phase for each, as the feedback gain is increased. The jet distribution again performs most favorably since the disturbance rotation rate is reduced as the feedback gain is increased. Note that the rotation rate of the disturbance wave is dependent on the gain and phase of the feedback signal, and the dependence of rotation speed on gain shown in the figure holds for the optimum phase based on range extension at the particular operating point that was chosen. For a particular operating point one could also optimize the phase of the actuation to produce the lowest rotation rate for the controlled disturbance. Even if feedback phase is optimized in this way, the trends shown in Fig. 9 hold, i.e., the jet actuator achieves lower disturbance rotation rates than do the other actuators.

Influence of Sensor

Sensing schemes were compared with the sensors located at various axial stations in the compression system for each

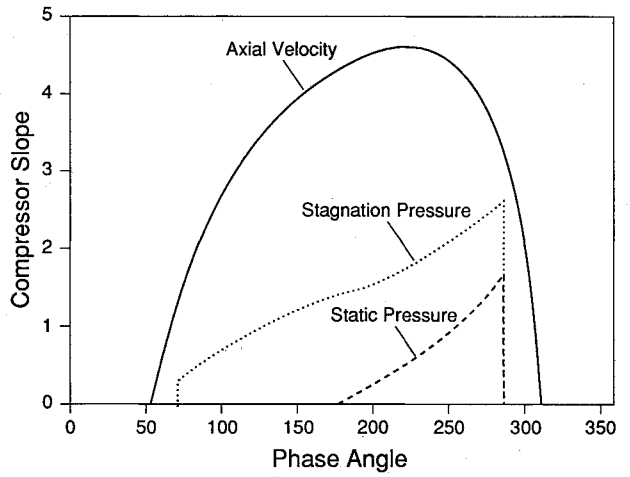

Fig. 10 Jet actuator with various sensors; neutral stability at a gain = 4.

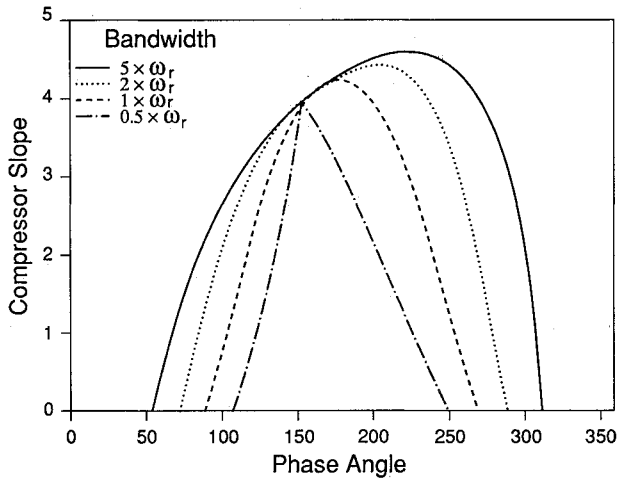

Fig. 11 Jet actuator; neutral stability as a function of actuator bandwidth.

of the actuators considered. Only the results for the jet actuator are presented here since it appears to be the most effective based on the performance criteria identified above, and the results for the other actuators are qualitatively similar. Figure 10 shows a comparison of the system performance with the various sensing schemes. In this figure the sensors are located at the axial station where they perform best; downstream of the actuator for axial velocity sensing (either upstream or downstream of the compressor), and downstream of the compressor for static and stagnation pressure sensing. From the figure it is apparent that the system performs best when axial velocity is sensed. While axial velocity is readily measured in low-speed flows with hot wires, these sensors are not practical in high-speed turbomachinery. Here, velocity could be synthesized from total and static pressure measurements.

There are indications that the disappointing performance of the pressure sensors could be a result of the simple proportional feedback law that was used. The system performance could possibly be improved if dynamic compensation is used in the feedback loop, but this was not pursued in the study.

Influence of Actuator Bandwidth

For the results that have been presented thus far, a bandwidth of five times the rotor frequency has been used to compare the actuators and sensors operating as close as possible to ideal. This actuator bandwidth might be difficult to achieve in practice. Figure 11 shows a comparison of the

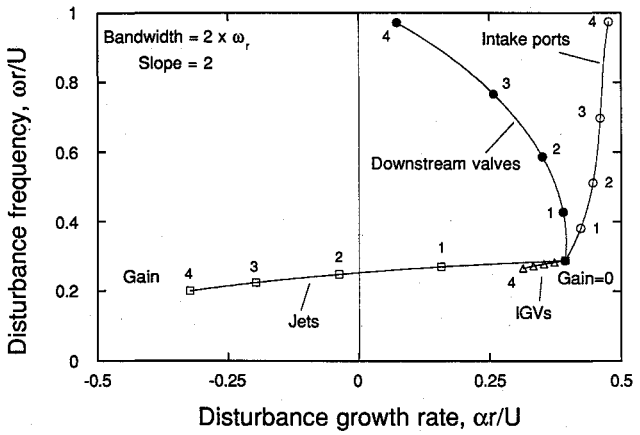

Fig. 12 Perturbation growth and rotation rates (bandwidth = 2 × rotor frequency).

performance of the jet actuator for various bandwidths, from five times rotor frequency down to 50% of rotor frequency. The major effect of decreasing the bandwidth is narrowing of the phase margin of the actuation system. The range extension gained from the actuator is affected less severely by narrower actuator bandwidths.

The other actuators are impacted more severely by a decrease in actuator bandwidth than is the jet actuator, as seen in Fig. 12. The plot is similar to Fig. 9, except that the actuator bandwidth has been decreased from five times to twice rotor frequency. Because the rotational frequency of the controlled disturbance is small in the case of the jet actuator, the increased time delay corresponds to a small additional spatial phase shift between the sensed and the actuated waves, so the effect on the stability of the wave is relatively small. With the valve and intake port actuators, the frequency of the controlled wave increases significantly as the gain is increased, as seen in Fig. 9. An increase in actuator time delay therefore increases the spatial phase shift between the sensed and actuated waves significantly. In addition, from Fig. 8, it is evident that the range of phases over which these controlled systems are stable is significantly smaller than in the case of the jet actuator. The additional spatial phase shift in the actuation which results from the increased time delay moves the system outside the area of previously stable operation. This is clear if one compares Fig. 12 to Fig. 9. The effects of time delays can probably be decreased if suitable dynamic compensation is used in the feedback loop, but this has not been pursued in the present study.

Conclusions

The model that has been used in this study captures the behavior of the rotating stall disturbance waves that have been observed in experiments. The quantitative agreement of the model with the experiments gives us confidence in using the modeling technique in the analysis of the controlled compressors considered in the study. This theoretical analysis indicates that a circumferential array of jets upstream of the compressor performs significantly better than the other actuators that were considered, in all of the performance criteria that were identified. In addition to providing the maximum range extension, jets also outperform the other actuators that were considered in other areas that would be important in practical applications. The large phase margin associated with jet actuation implies that the system will not be sensitive to errors in disturbance wave measurement. The jet actuator decreases the rotation rate of disturbances and this alleviates the high bandwidth requirement of some of the other actuators. One may, however, incur an efficiency penalty when the jet actuator is used because of the high-pressure air supply required. This penalty is incurred only if the compressor is operated in the previously unstable flow range. Whether this efficiency penalty is acceptable or not depends on the design goals of the compressor.

The results of the study also indicate that velocity sensing is more effective than either static or total pressure sensing in controlling rotating stall disturbances, for the proportional control law that was considered. In low-speed compressors velocity sensing with hot wire probes is effective, but in high-speed compressors the use of hot wires might not be practical. The velocity perturbation could then be synthesized from static and total pressure measurements.

The bandwidth requirement of actuators is important since it has a significant effect on the performance of the controlled system. For the jet actuator, the phase margin of the controlled system is degraded as the bandwidth of the actuator is reduced.

Finally, although the movable inlet guide vane actuator performed well in practice, it did not compare favorably with the other actuators that were considered in the theoretical study. The potential for compressor range extension is therefore much greater than that achieved thus far in the laboratory.

Appendix A: Overall Flow Model

The basic derivation of the flow has appeared before,[1-3] and is included for completeness. In the model the pressure rise across a compressor is modified by the pressure difference required to overcome the inertia of the fluid within the blade channels when the flow within the compressor is unsteady. If one assumes that the flow within the blade passages is one-dimensional, the unsteady pressure rise across the compressor can be written as[1,2,14]

$$\frac{P_e - P_{ti}}{\rho U^2} = \psi - \lambda \frac{\partial \phi}{\delta \vartheta} - \frac{\mu r}{U} \frac{\partial \phi}{\partial t} \tag{A1}$$

where

$$\psi = \psi_i - L_r - L_s \tag{A2}$$

The inertia of the fluid in the rotors and in the compressor are represented by λ and μ, respectively. At the inception of rotating stall, the flow coefficient through the compressor is modified by a small perturbation $\delta\phi$ so that

$$\begin{aligned} \phi &= \bar{\phi} + \delta\phi & \psi_i &= \bar{\psi}_i + \frac{\mathrm{d}\bar{\psi}_i}{\mathrm{d}\phi}\delta\phi \\ P_e &= \bar{P}_e + \delta P_e & L_s &= \bar{L}_s + \delta L_s \\ P_{ti} &= \bar{P}_{ti} + \delta P_{ti} & L_r &= \bar{L}_r + \delta L_r \end{aligned} \tag{A3}$$

The compressor pressure rise perturbation equation is therefore

$$\frac{\delta P_e - \delta P_{ti}}{\rho U^2} = \frac{\mathrm{d}\bar{\psi}_i}{\mathrm{d}\phi}\delta\phi - \delta L_s - \delta L_r - \lambda \frac{\partial(\delta\phi)}{\partial \vartheta} - \frac{\mu r}{U}\frac{\partial(\delta\phi)}{\partial t} \tag{A4}$$

$$\bar{\psi}_i = \bar{\psi} + \bar{L}_r + \bar{L}_s \tag{A5}$$

δL_s is taken to be given by the differential equation

$$\tau_s \frac{\partial(\delta L_s)}{\partial t} = \frac{\mathrm{d}\bar{L}_s}{\mathrm{d}\phi}\delta\phi - \delta L_s \tag{A6}$$

δL_r has to be calculated in a reference frame rotating with the rotor:

$$\tau_r \left[\frac{\partial(\delta L_r)}{\partial t} + \frac{U}{r}\frac{\partial(\delta L_r)}{\partial \vartheta}\right] = \frac{\mathrm{d}\bar{L}_r}{\mathrm{d}\phi}\delta\phi - \delta L_r \tag{A7}$$

In the analysis, a general perturbation in flow coefficient of the form

$$\delta\phi = \sum_{n=1}^{\infty} A_n e^{(\alpha_n + i\omega_n)t} e^{in\vartheta} \tag{A8}$$

is considered. Each spatial harmonic of the perturbation can be considered separately and only the nth spatial harmonic

$$\delta\phi = A_n e^{(\alpha_n + i\omega_n)t} e^{in\vartheta} \tag{A9}$$

will therefore be examined.

The variables describing the evolution of the perturbation can be nondimensionalized as follows:

$$\bar{t} = \frac{tU}{r}$$

$$\bar{\tau} = \frac{\tau U}{r} \tag{A10}$$

$$s = \frac{(\alpha_n + i\omega_n)r}{u}$$

where U is the rotor speed, so that the equations describing the perturbation become

$$\frac{\delta P_e - \delta P_{ti}}{\rho U^2} = \frac{d\bar{\psi}_i}{d\phi}\delta\phi - \delta L_s - \delta L_r - \lambda\frac{\partial(\delta\phi)}{\partial\vartheta} - \mu\frac{\partial(\delta\phi)}{\partial\bar{t}} \tag{A11}$$

$$\bar{\tau}_s\frac{\partial(\delta L_s)}{\partial\bar{t}} = \frac{d\bar{L}_s}{d\phi}\delta\phi - \delta L_s \tag{A12}$$

$$\bar{\tau}_r\left[\frac{\partial(\delta L_r)}{\partial\bar{t}} + \frac{\partial(\delta L_r)}{\partial\vartheta}\right] = \frac{d\bar{L}_r}{d\phi}\delta\phi - \delta L_r \tag{A13}$$

$$\delta\phi = A_n e^{s\bar{t}} e^{in\vartheta} \tag{A14}$$

The upstream stagnation and downstream static pressure perturbations are given by the expressions[3]

$$\frac{\delta P_{ti}}{\rho U^2} = -\frac{1}{|n|}\frac{\partial(\delta\phi)}{\partial\bar{t}} \tag{A15}$$

$$\frac{\delta P_e}{\rho U^2} = \frac{1}{|n|}\frac{\partial(\delta\phi)}{\partial\bar{t}} \tag{A16}$$

Substitution of Eqs. (A15), (A16), and (A14) into Eqs. (A11–A13) produces a generalized, complex eigenvalue problem in s

$$(A - sB)\delta\bar{x} = 0 \tag{A17}$$

where

$$A = \begin{bmatrix} \frac{1}{\zeta}\left(\frac{d\bar{\psi}_i}{d\phi} - in\lambda\right) & -\frac{1}{\zeta} & -\frac{1}{\zeta} \\ \frac{1}{\bar{\tau}_s}\frac{d\bar{L}_s}{d\phi} & -\frac{1}{\bar{\tau}_s} & 0 \\ \frac{1}{\bar{\tau}_r}\frac{d\bar{L}_r}{d\phi} & 0 & -\left(in + \frac{1}{\bar{\tau}_r}\right) \end{bmatrix} \tag{A18}$$

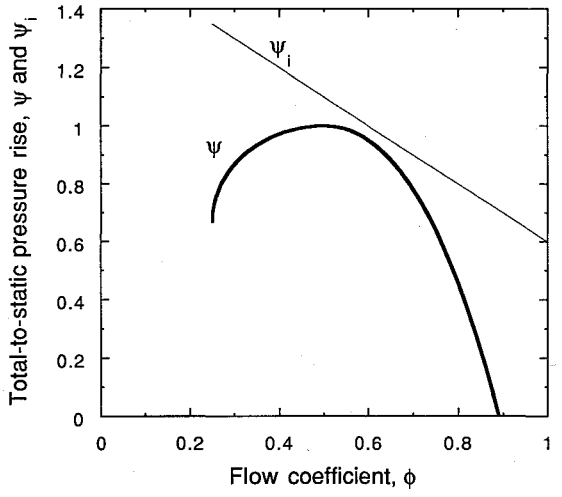

Fig. A1 Compressor total-to-static characteristics used in the analysis.

$$B = \begin{pmatrix} 1 & 0 & 0 \\ 0 & 1 & 0 \\ 0 & 0 & 1 \end{pmatrix} \tag{A19}$$

$$\delta\bar{x} = \begin{pmatrix} \delta\phi \\ \delta L_s \\ \delta L_r \end{pmatrix} \tag{A20}$$

$$\zeta = \left(\frac{2}{|n|} + \mu\right) \tag{A21}$$

$$\psi_i = \bar{\psi} + \bar{L}_s + \bar{L}_r \tag{A22}$$

The solution to the eigenvalue problem yields the growth and rotation rates of the perturbation wave.

To determine the unsteady response of the compressor to flow perturbations, an isentropic pressure rise characteristic for the compressor has to be assumed. For the analysis it is assumed that the compressor operates at its maximum efficiency at a flow coefficient of 0.6. At this maximum efficiency operating point, the slope of the isentropic pressure rise characteristic is close to that of the measured pressure rise characteristic, since the losses are minimum. To simplify the analysis, the isentropic characteristic is assumed to have this slope over the entire operating range of the compressor as shown in Fig. A1. The steady total pressure loss [$\bar{L}(\phi) = \bar{L}_r(\phi) + \bar{L}_s(\phi)$] used in Eq. (A5) is then the difference between the isentropic pressure rise curve and the measured one. In the analysis it is also assumed that steady total pressure losses are equally distributed across the rotors and the stators (i.e., $\bar{L}_r = \bar{L}_s$).

Appendix B: Modification of the Flow Model for Active Control

In an actively controlled compressor, the relation between pressure and velocity perturbations can be manipulated by the actuator. Quasisteady actuator disk theory is used to determine the relation between actuation and the perturbations introduced into the flowfield. The upstream jet distribution will be used as an example to illustrate the analysis method. A mass balance across the actuator gives

$$\rho(c_x + \delta c_{x1})l_a + \rho c_{xj}\delta l_j = \rho(c_x + \delta c_{x2})l_a \tag{B1}$$

and nondimensionalizing the velocities by U yields

$$\delta\phi_2 = \delta\phi_1 + \phi_j\frac{\delta l_j}{l_a} \tag{B2}$$

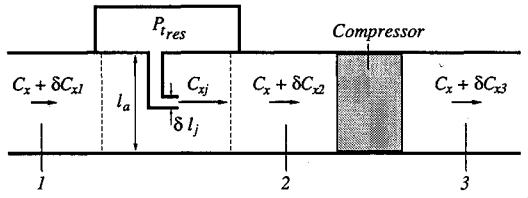

Fig. B1 Jet actuator.

The nondimensionalized injection rate $\phi_j(\delta l_j/l_a)$ is a function of the annulus spatial variable ϑ. The nondimensionalized injection axial velocity ϕ_j, the jet nozzle opening δl_j, and l_a, are indicated in Fig. B1.

A momentum balance across the actuator gives

$$\rho(c_x + \delta c_{x1})^2 l_a + (P + \delta P_1) l_a + \rho c_{xj}^2 \delta l_j = \rho(c_x + \delta c_{x2})^2 l_a + (P + \delta P_2) l_a \tag{B3}$$

If only first-order terms are retained, the above expression can be written in terms of total pressure perturbations upstream of the actuator and at the compressor face

$$\frac{\delta P_{t2}}{\rho U^2} = \frac{\delta P_{t1}}{\rho U^2} + (\phi_j - \phi)\phi_j \frac{\delta l_j}{l_a} \tag{B4}$$

The downstream static pressure perturbation is given by expression (A16). It is apparent from (B1) and (B4) that the compressor inlet total pressure and flow coefficient perturbations can be controlled by specifying $\phi_j(\delta l_j/l_a)$, the annular injection rate of jet fluid into the airstream.

Control is accomplished by sensing a fluid dynamic variable describing the perturbation. The measured signal is then processed by the controller which commands the actuator to introduce a suitable perturbation into the flowfield. In the simplest controller, the measured signal is modified in amplitude and shifted spatially in phase (proportional feedback). This is implemented analytically as follows; if the flow coefficient perturbation at the compressor face is sensed, the commanded jet injection rate is

$$\phi_j \frac{\delta l_j}{l_a}\bigg|_c = Z\delta\phi_2 \tag{B5}$$

$$Z = Re^{i\vartheta_a} \tag{B6}$$

where R is the gain in amplitude of the signal, and ϑ_a is the spatial phase shift of the commanded signal relative to the measured signal. In practice, nonideal behavior will cause the output from the actuator to differ from the command given by the controller. To capture the nonideal dynamics, the actuator is modeled as a first-order system

$$\bar{\tau}_a \frac{\partial}{\partial \bar{t}}\left(\phi_j \frac{\delta l_j}{l_a}\right) = \phi_j \frac{\delta l_j}{l_a}\bigg|_c - \phi_j \frac{\delta l_j}{l_a} \tag{B7}$$

where $\bar{\tau}_a$ is the time constant associated with the actuator. If the flow coefficient (axial velocity) at the compressor face is sensed, the actuator equation becomes

$$\bar{\tau}_a \frac{\partial}{\partial \bar{t}}\left(\phi_j \frac{\delta l_j}{l_a}\right) = Z\delta\phi_2 - \phi_j \frac{\delta l_j}{l_a} \tag{B8}$$

Sensing the other fluid dynamic variables gives the following actuator commands:

stagnation pressure upstream of the actuator

$$\phi_j \frac{\delta l_j}{l_a}\bigg|_c = Z\frac{\delta P_{t1}}{\rho U^2} = -Z\frac{s}{|n|}\left(\delta\phi_2 - \phi_j \frac{\delta l_j}{l_a}\right) \tag{B9}$$

static pressure upstream of the actuator

$$\phi_j \frac{\delta l_j}{l_a}\bigg|_c = Z\frac{\delta P_1}{\rho U^2} = -Z\left(\frac{s}{|n|} + \phi\right)\left(\delta\phi_2 - \phi_j \frac{\delta l_j}{l_a}\right) \tag{B10}$$

exit static pressure

$$\phi_j \frac{\delta l_j}{l_a}\bigg|_c = Z\frac{\delta P_3}{\rho U^2} = Z\frac{s}{|n|}\delta\phi_2 \tag{B11}$$

exit stagnation pressure

$$\phi_j \frac{\delta l_j}{l_a}\bigg|_c = Z\frac{\delta P_{t3}}{\rho U^2} = Z\left(\frac{s}{|n|} + \phi\right)\delta\phi_2 \tag{B12}$$

which, when substituted into Eq. (B7), yield equations similar to Eq. (B8).

Equations (A11–A13) and Eq. (B7) with the appropriate sensed variable produce an eigenvalue problem. Parameters in the analysis are the operating flow coefficient (which determines the slope of the pressure rise characteristic), the gain and phase of the feedback control law, and the bandwidth of the actuator. For the jet distribution with velocity feedback, the system of differential equations reduces to the form given in (A17), where the matrices A, B, and the vector $\delta\bar{x}$ are now

$$A = \begin{bmatrix} \frac{1}{\zeta}\left(\frac{d\bar{\psi}_i}{d\phi} - in\lambda\right) & -\frac{1}{\zeta} & -\frac{1}{\zeta} & \frac{1}{\zeta}(\phi_j - \phi) \\ \frac{1}{\bar{\tau}_s}\frac{d\bar{L}_s}{d\phi} & -\frac{1}{\bar{\tau}_s} & 0 & 0 \\ \frac{1}{\bar{\tau}_r}\frac{d\bar{L}_r}{d\phi} & 0 & -\left(in + \frac{1}{\bar{\tau}_r}\right) & 0 \\ \frac{1}{\bar{\tau}_a}Z & 0 & 0 & -\frac{1}{\bar{\tau}_a} \end{bmatrix} \tag{B13}$$

$$B = \begin{bmatrix} 1 & 0 & 0 & -\frac{1}{|n|\zeta} \\ 0 & 1 & 0 & 0 \\ 0 & 0 & 1 & 0 \\ 0 & 0 & 0 & 1 \end{bmatrix} \tag{B14}$$

$$\delta_{\bar{x}} \begin{bmatrix} \delta\phi_2 \\ \delta L_s \\ \delta L_r \\ \phi_j \frac{\delta l_j}{l_a} \end{bmatrix} \tag{B15}$$

There are four eigenvalues for each spatial harmonic of the disturbance.

Acknowledgments

This work has been supported by the U.S. Air Force Office of Scientific Research, D. Fant technical monitor, and the Government Engine and Space Propulsion Division of Pratt & Whitney/United Technologies, S. Baghdadi and J. Garberoglio technical monitors. Financial support for D. L. Gysling was provided by the Air Force Research in Aero Propulsion Technology (AFRAPT) program. The authors wish to thank E. M. Greitzer, A. H. Epstein, J. D. Paduano, J. S. Simon, and J. M. Haynes for many useful discussions.

References

[1]Moore, F. K., "A Theory of Rotating Stall of Multistage Axial Compressors: Part 1—Small Disturbances," *Journal of Engineering for Gas Turbines and Power*, Vol. 106, April 1984, pp. 313–320.

[2]Hynes, T. P., and Greitzer, E. M., "A Method for Assessing Effects of Circumferential Flow Distortion on Compressor Stability," *Journal of Turbomachinery*, Vol. 109, July 1987, pp. 371–379.

[3]Epstein, A. H., Ffowcs Williams, J. E., and Greitzer, E. M., "Active Suppression of Aerodynamic Instabilities in Turbomachines," *Journal of Propulsion and Power*, Vol. 5, No. 2, 1989, pp. 204–211.

[4]Garnier, V. H., Epstein, A. H., and Greitzer, E. M., "Rotating Waves as a Stall Inception Indication in Axial Compressors," *Journal of Turbomachinery*, Vol. 113, April 1991, pp. 290–301.

[5]McDougal, N. M., Cumpsty, N. A., and Hynes, T. P., "Stall Inception in Axial Compressors," *Journal of Turbomachinery*, Vol. 112, Jan. 1990, pp. 116–125.

[6]Day, I. J., "Stall Inception in Axial Flow Compressors," *Journal of Turbomachinery*, Vol. 115, Jan. 1993, pp. 1–9.

[7]Paduano, J. D., "Active Control of Rotating Stall in Axial Compressors," Ph.D. Dissertation, Massachusetts Inst. of Technology, Dept. of Aeronautics and Astronautics, Cambridge, MA, Nov. 1991.

[8]Paduano, J., Epstein, A. H., Valavani, L., Longley, J. P., Greitzer, E. M., and Guenette, G. R., "Active Control of Rotating Stall in a Low Speed Axial Compressor," American Society of Mechanical Engineers, Paper 91-GT-88, June 1991.

[9]Haynes, J. M., "Active Control of Rotating Stall in a Three-Stage Axial Compressor," M.S. Thesis, Dept. of Mechanical Engineering, Massachusetts Inst. of Technology, Cambridge, MA, Sept. 1992.

[10]Nagano, S., Machida, Y., and Takata, H., "Dynamic Performance of Stalled Blade Rows," Japan Society of Mechanical Engineering Paper JSME 11, Tokyo, Japan, Oct. 1971.

[11]Mazzawy, R. S., "Multiple Segment Parallel Compressor Model for Circumferential Flow Distortion," *Engineering for Power*, Vol. 99, No. 2, 1977, pp. 288–296.

[12]Greitzer, E. M., et al., "Dynamic Control of Aerodynamic Instabilities in Gas Turbine Engines," AGARD Lecture Series on Steady and Transient Performance Prediction of Gas Turbine Engines, Cambridge, MA, May 1992.

[13]Gysling, D. L., "Dynamic Control of Rotating Stall in Axial Flow Compressors Using Aeromechanical Feedback," Ph.D. Dissertation, Massachusetts Inst. of Technology, Dept. of Aeronautics and Astronautics, Cambridge, MA (to be published).

[14]Chue, R., Hynes, T. P., Greitzer, E. M., Tan, C. S., and Longley, J. P., "Calculations of Inlet Distortion Induced Compressor Flow Field Instability," *International Journal of Heat and Fluid Flow*, Vol. 10, No. 3, Sept. 1989, pp. 211–223.